



THE UNIVERSITY OF  
**SYDNEY**

SCHOOL OF AEROSPACE MECHANICAL AND MECHATRONIC ENGINEERING

AERO3760: SPACE ENGINEERING 2

---

## Group E: SnapSat

### Data Package Document 1 Critical Design Review

---

21 AUGUST 2015

Name and Email	Role and Responsibility
James Allworth   312073038 jall8741@uni.sydney.edu.au	<i>Attitude Determination and Control System</i> TASKS
Thomas Forbutt   312101058 tfor8012@uni.sydney.edu.au	<i>Communications and Data Handling</i> TASKS
Oscar McNulty   312106130 omcn3220@uni.sydney.edu.au	<i>Structural Design and Development</i> TASKS
Penelope Player   312106718 ppla7388@uni.sydney.edu.au	<i>On-board Computer and Power System</i> TASKS
Nikita Sardesai   312088205 nsar2497@uni.sydney.edu.au	<i>Thermal System Design and Payload</i> TASKS

# Contents

<b>1 System Overview . . . . .</b>	<b>4</b>
1.1 Mission and Objectives . . . . .	4
1.2 Components and Subsystems . . . . .	4
1.3 System Integration . . . . .	5
<b>2 Payload Design . . . . .</b>	<b>6</b>
2.1 Integration . . . . .	6
<b>3 Structural Subsystem . . . . .</b>	<b>7</b>
<b>4 Attitude Determination and Control Subsystem . . . . .</b>	<b>8</b>
4.1 Location and Attitude Determination . . . . .	8
4.1.1 Global Positioning System . . . . .	8
4.1.2 Inertial Measurement Unit . . . . .	8
4.1.3 Photodiode Sun Sensor System . . . . .	8
4.2 Attitude Control System . . . . .	9
4.2.1 Selection of Magnetorquers . . . . .	9
4.2.2 Design of Magnetorquer . . . . .	10
4.2.3 Construction of Magnetorquers . . . . .	11
4.3 Control System . . . . .	13
4.3.1 Detumble Phase . . . . .	13
4.3.2 Attitude Control Phase . . . . .	13
4.3.3 Single Axis Control Model . . . . .	14
4.4 Disturbance Torques . . . . .	16
<b>5 Electrical Power Subsystem . . . . .</b>	<b>17</b>
5.1 Charging Circuit . . . . .	17
5.2 Voltage Rails . . . . .	17
5.3 Battery Lifetime . . . . .	18
<b>6 On-Board Computer and On-board Data Handling Subsystem . . . . .</b>	<b>19</b>
6.1 Selection . . . . .	19
6.2 On-board Data Handling . . . . .	19
6.3 Modes of Operation . . . . .	19
<b>7 Communications Subsystem . . . . .</b>	<b>21</b>
7.1 Componenets . . . . .	21
Ground Station . . . . .	26
7.2 Link Budget Summary . . . . .	26
<b>8 Thermal Control Subsystem . . . . .</b>	<b>28</b>
8.1 The Three Modes of Heat Transfer . . . . .	28
8.1.1 Convection . . . . .	29
8.1.2 Conduction . . . . .	29
8.1.3 Radiation . . . . .	29
8.2 Total Incoming Radiation . . . . .	29

8.2.1	View Factors . . . . .	30
8.3	Spacecraft Thermal Environment . . . . .	31
8.3.1	Solar Radiation . . . . .	31
8.3.2	Earth Infrared Radiation . . . . .	32
8.3.3	Earth Albedo . . . . .	32
8.3.4	Total Incoming Radiation Per Panel . . . . .	33
<b>A</b>	<b>Link Budgets . . . . .</b>	<b>35</b>

## List of Figures

1.1	Full System Integration . . . . .	5
2.1	An image of the ArduCAM Mini. Note that there is no storage mechanism on this module, necessitating an external SD card. . . . .	6
2.2	The SD card used in SnapSat . . . . .	6
4.1	Sun Vector in a Plane [1] . . . . .	9
4.2	Comparison of Control Systems for Current Satellites [2] . . . . .	10
4.3	Magnetorquer Construction Set Up . . . . .	12
4.4	Completed Magnetorquer . . . . .	13
4.5	Model of Kalman Filter [?]. . . . .	14
4.6	Simulink Model of Yaw Axis Control System . . . . .	15
4.7	Yaw Angle Rotation to 90° . . . . .	15
5.1	The EPS PCB. Although this PCB is full it is functional, and the extra changing circuit has not taken the place of another component. . . . .	17
6.1	A diagram showing the interactions between the MCU and the other subsystems. .	19
6.2	A diagram showing the modes of operation during flight. . . . .	20
7.1	RFD900 . . . . .	21
7.2	Pin Diagram . . . . .	22
7.3	Table of pins used . . . . .	22
7.4	Settings used with transciever . . . . .	24
7.5	Quarter Wave Monopole Antenna . . . . .	25
7.6	Five-node Network Setup . . . . .	26
7.7	Uplink budget . . . . .	27
7.8	Downlink budget . . . . .	27
8.1	Incoming thermal radiation on the satellite . . . . .	28
8.2	Radiation incoming onto the satellite as it orbits . . . . .	30
8.3	Representation of Satellite Orbit . . . . .	31
8.4	Solar radiation falling on each panel . . . . .	32
8.5	Reflected albedo falling on each panel . . . . .	33
8.6	Total radiation falling upon panel 2 . . . . .	33
A.1	Uplink budget . . . . .	35
A.2	Downlink budget . . . . .	36

## List of Tables

1.1	Overview of component selection . . . . .	5
-----	---	---

4.1	Predicted Data for the Magnetorquers . . . . .	11
4.2	Estimated Disturbance Torques on SnapSat . . . . .	16

# 1 System Overview

*SnapSat* is an undergraduate project taken on by five students at the University of Sydney. The report will detail the Critical Design Review and specifications that were built to over the 12 week semester. The details of the subsystems and the system integration will be detailed here. The initial design point was for a three month mission at an orbit altitude of 350 kilometres and an inclination of 98°. However, this report will mainly detail the requirements for a 30km high-altitude balloon launch. Recommendations and upgrades to make this project viable for the initial design point will be made appropriately.

## 1.1 Mission and Objectives

The main mission of *SnapSat* is to provide a platform to make space activities more accessible to the general public. The aim is to exploit popular social media and to allow the end user to post Twitter updates (Tweets) along with photographs of the Earth from the satellite. In order to do this, the cubesat needs a camera with sufficient resolution to see general country regions (and possible cities) along with a reliable communications connection to allow for fast data transfer at an orbit altitude of 350 kilometres.

## 1.2 Components and Subsystems

On a primary level, for the design on a high-altitude balloon, the main payload is the camera. Other basic requirements for the launch (power and communications) will be outlined in the following sections and discussed in detail later on in the report. An Attitude Determination and Control Subsystem (ADCS) was also tested and implemented as a proof-of-concept. The full structure was designed in-house and was a conventional laser-cut aluminium chassis. Details of the subsystems and the components chosen to meet each task are detailed in table 1.1 below. The budget for the project was \$1000 provided by the School of Aerospace, Mechanical and Mechatronic Engineering at the University of Sydney. Components were selected based on their suitability for the project and for their cost. It was also important to take into consideration the working of other teams within the course. The communications structure chose relies on a ‘mother’ satellite, through which all communications are managed. Components were selected to allow for this to work effectively. The purpose of having a mother satellite was to allow for an easy find after the high altitude balloon launch.

Table 1.1: Overview of component selection

Subsystem	Chosen Components
Structural	- industrial grade Aluminium - laser cut, bent to shape and riveted together with M3 threaded rods to supports the Printed Circuit Boards (PCBs)
ADCS	- air-core magnetorquers designed and made in house - OSRAM SFH203P photodiodes to track Sun location - Inertial Measurement Unit (IMU) to obtain gyroscopic data: Adafruit 10-DOF
EPS	- 9cm × 9cm solar panels - 2 × LiNiMnCo 26650 rechargeable cells - Adafruit voltage regulators
OBC/OBDH	- Microcontroller: Iduino DUE (Arduino DUE clone) - PCB × 4: power board, control systems and payload board, communications board, microcontroller board
TT&C	- RF 900 chip - duck antennae - Ublox 3.3V GPS
Thermal	- passive coatings on cubesat chassis: kapton tape
Payload	- camera: Arducam mini

### 1.3 System Integration

Figure 1.1 below shows the schematic of how all the subsystems will work together and their communication protocol.

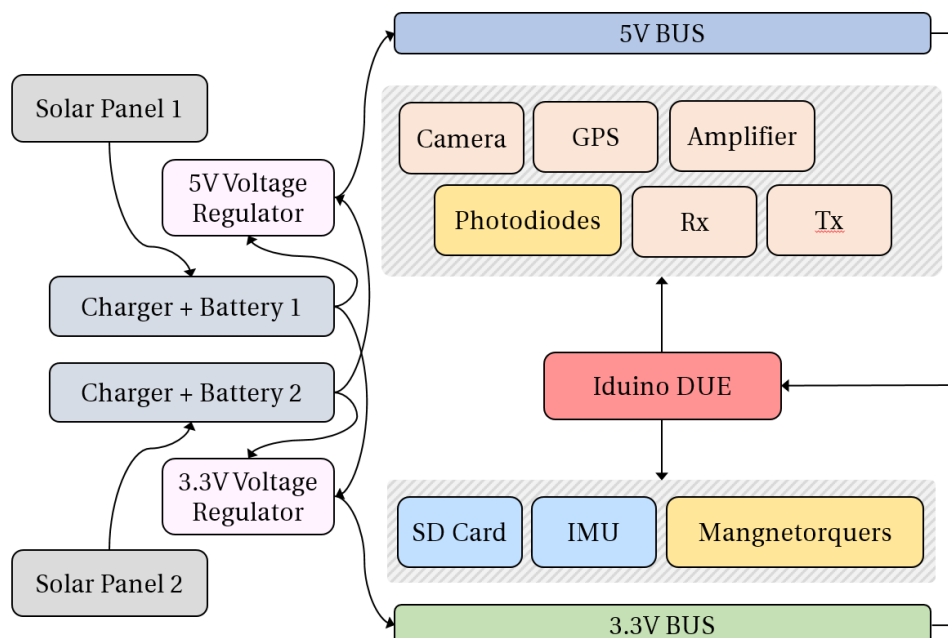


Figure 1.1: Full System Integration

## 2 Payload Design

The SnapSat payload is a single camera, used to take images of the earth throughout the flight. Due to the inherent size and power limitation of CubeSats, budget and ease of interface with the Iduino Due Pro, the 2MP ArduCAM Mini was selected.

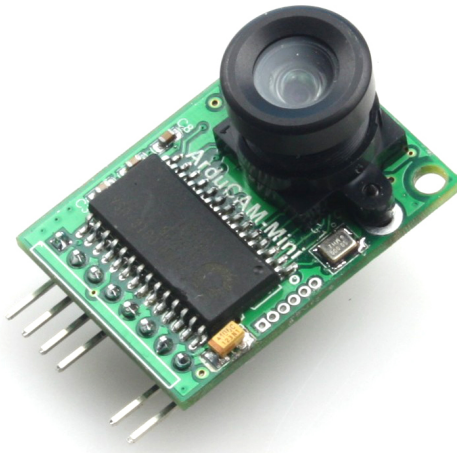


Figure 2.1: An image of the ArduCAM Mini. Note that there is no storage mechanism on this module, necessitating an external SD card.

Unlike the ArduCAM, on which this is based, the ArduCAM mini has no integrated SD Card to store photos. As such, the design includes an Adafruit SD Card which stores all pictures.

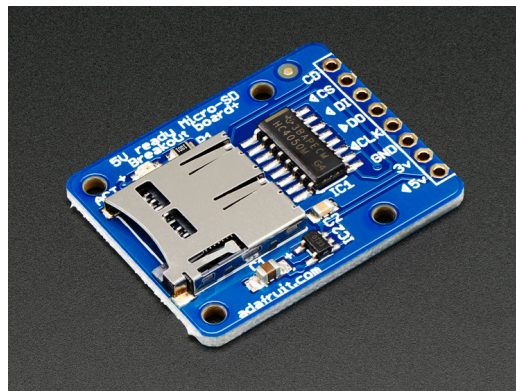


Figure 2.2: The SD card used in SnapSat

### 2.1 Integration

These two devices operate off the one SPI module and are physically located on the Bottom PCB. Additionally, the ArduCAM mini image sensor is controlled through I2C1 module. Both devices are powered by the 5V line, and use 3.3V CMOS logic levels, with no step up required.

STICK IN IMAGE OF BOTTOM PCB COMPLETED

Ultimately using a 16GB SD Card, assuming a size of 1MB per photo, and a balloon flight time of 4 hours this module is able to record 16000 photos or a photo every second.

### **3 Structural Subsystem**

## 4 Attitude Determination and Control Subsystem

### 4.1 Location and Attitude Determination

#### 4.1.1 Global Positioning System

The SnapSat uses a GPS to determine its latitudinal and longitudinal position above the surface of the earth. An Adafruit Ultimate GPS Breakout Version 3 which has an attitudinal limit of 40km was selected for the balloon launch. As this GPS only has a rating up to 40km it will not be suitable for a space mission.

#### 4.1.2 Inertial Measurement Unit

The inertial measurement unit (IMU) that was selected for the balloon launch is a 10 degree of freedom (DOF) Adafruit IMU. It includes a 3DOF magnetometer, a 3D0F accelerometer and a 3DOF gyroscope as well as a barometric pressure/altitude sensor which also includes temperature. The IMU uses an Attitude Heading and Reference System (AHRS) algorithm that returns the pitch, yaw and roll of the satellite with respect to magnetic north. Given the fact that this is a very cheap IMU there is a degree of drift associated with the gyroscope which causes inaccuracies. There is also an error associated with the accelerometer however it is less than the the drift caused by the gyroscope. As such the accelerometer has been used to determine the attitude both for the balloon launch and in the functional testing as the photodiode system will not be functional in either of these tests.

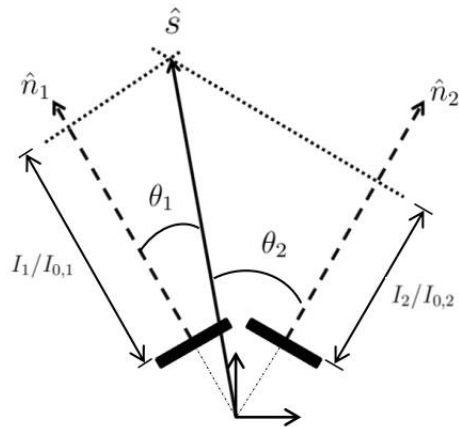
In terms of the application in space for this component, the major problem with this IMU is that it is not radiation hardened which will result in larger errors the longer it remains in orbit and will eventually cause it to stop working. Thus in the event of an actual space launch, this component would need to be replaced with a radiation and preferably more accurate component. The other major error that effects the IMU is accumulated error which is directly related to the amount of time spent in orbit. Although this may be reduced in higher quality IMU's it will always be an issue. Thus a secondary orientation system is required in order to determine the attitude of the SnapSat accurately.

#### 4.1.3 Photodiode Sun Sensor System

A photodiode based sun sensor system was selected to be the secondary orientation system in order to recalibrate the IMU and to use in long duration missions. This system was primarily selected because it provides enough pointing accuracy for the purposes of this mission and is significantly cheaper than the alternatives of star trackers or actual sun sensors. The actual component that was selected is an OSRAM SFH203P Photodiode. Although these are simply off the shelf components, a cover glass can be placed over the photodiodes in order to protect them from UV radiation.

There are two common methods for placing photodiodes on a cubesat. The first is to use six photodiodes that are orthogonal, one for each side. However this method does not provide photodiode coverage sufficient for sun vector estimation over the entire attitude sphere because the field of view of individual photodiodes is generally less than 180°. The second method is to place pairs of photodiodes angled in a single plane which allows the sun vector component in the common plane to be measured as shown in the figure below:

Figure 4.1: Sun Vector in a Plane [1]



The three axis vector is then formulated by finding the intersection of multiple planes. For the space launch of SnapSat, the second method will be utilised in order to enable attitude calculation throughout the entire attitude sphere during orbit. Photodiodes output current as a function of the light intensity and angle to the light source. Thus utilising the information from the photodiodes a three dimensional sun vector can be created using the following equation [3]: The photodiode system has limitations caused by occlusion, which is when the sensor's view of the Sun is blocked and albedo, which is when reflected sunlight from the earth or the moon distorts the reading. [4]

## 4.2 Attitude Control System

### 4.2.1 Selection of Magnetorquers

The SnapSat is a 1kg cubesat with low mass, power and budget considerations. Subsequently, given these constraints, it was determined that magnetorquers would be the simplest and most cost efficient way to control the satellite. To determine a rough estimate for the system requirements and available options, the magnetorquers for a number of similar cubesats were compared, as can be seen in the table below:

Figure 4.2: Comparison of Control Systems for Current Satellites [2]

Mission	Type	Magnetic Moment (A·m <sup>2</sup> )	Power (mW)	Mass (g)	Size	Notes
AAUSat	Air Core		122	20	8cmx9cm	X-Sec A=10mm <sup>2</sup> , C=356mm, R=100 ohms, Vbus=10V
AAUSat-3	Iron Core	0.03	6.8	19	200	XXX
CanX 2	3 Air Cores	0.1	40	100	XXX	5-35°C, built own winder
COMPASS-1	Air Core	0.085	26	19.2	400 turns	XXX
U Toronto GNB	Air Core	0.19	26	104	210 turns	XXX
GNB (2)	XXX	0.19	21	108	235 turns	XXX
Illinois, ION	Air Core	0.149	100	XXX	1500 turns	1.32e-8 m <sup>2</sup> X-sectional area, f Belden heavy armored poly-thermaleze 38 AWG
Illinois, TinySat	PCB Traced	XXX	114mA	XXX	120 loops	R=96.3Ω, 0.0007 in wire
CalPoly PolySat	PCB Traced		300mA		54 turns	0.1503 m <sup>2</sup>
Cute 1.7	3 Air Core	0.15	91	5	58.5 x 78.3 mm	2U Cubesat, 1 coil, 13mA drive current
SwissCube	3 Air Core	0.0285	XXX	XXX	XXX	Bdot and LQR
ISIS	Alloy Core	0.2	200	30	7 cm x 1 cm	-35 to 75°C, 1200
CubeTorquer	Iron Core	0.2	209	22	6 cm x 1 cm	Supra50 core, 1200 Euro

Using the comparison with the control systems for current satellites, it was determined that the SnapSat would require magnetorquers of approximately 0.1 to 0.15 Am<sup>2</sup>. Due to the need to be designed and built in house an air core magnetorquer was selected rather than iron or alloy core. To control the satellite attitude in all three axis, the SnapSat will require three separate magnetorquers, one for each axis. To further reduce power requirements the attitude control system will be set up so that only two of the magnetorquers can be turned on at any one time. This will allow each individual magnetorquer to use more power and as such draw a higher current than would otherwise have been the case.

#### 4.2.2 Design of Magnetorquer

The torque on the satellite produced by the magnetorquer is given by cross product of the magnetic dipole of the magnetorquer and the earth's magnetic field strength:

$$T = M \times B$$

It is impossible to change the earth's magnetic field strength which is approximately  $3 \times 10^{-6}$  Tesla. Thus in order to maximise the torque on the satellite the magnetic dipole must be maximised. The magnetic dipole for the magnetorquer is given by the following equation:

$$M = N \cdot I \cdot A$$

Thus the magnetic dipole is dependent on the number of turns in the coil, the current through the wire and the area of the coil. Initially it seems like a simple problem where the dipole will simply increase with the number of turns if the current and area are held constant. However, this view does not take into account the resistance that increases with the length of wire, which given the fixed voltage will limit the current. Due to cost restrictions, only 0.18mm round copper wire was available for use, which had a resistance per metre ( $R_m$ ) of 0.646 ohms. The following equations were then combined with the magnetic dipole equation in order to optimise the number of turns required:

$$I = \frac{V}{R}$$

$$R = N \cdot \text{Perimeter} \cdot R_m$$

$$P = V \cdot I$$

When combined the following equation was determined:

$$1 = \frac{4 \cdot M \cdot R_m}{V \cdot A}$$

Thus since resistance per metre and voltage are constant, and perimeter is dependent on area, the magnetic dipole becomes constant for a given area. Due to the restrictions in the lab only two sizes were available for the magnetorquers. The larger size was selected with side lengths of 0.073m as when the smaller size was modelled, the current draw was too high causing a higher level of power to be used. Thus given this fixed area, the maximum magnetic dipole was determined to be  $0.14Am^2$ . Using this maximum dipole as the basis, the other characteristics of the magnetorquer were determined and can be viewed in the table below.

Table 4.1: Predicted Data for the Magnetorquers

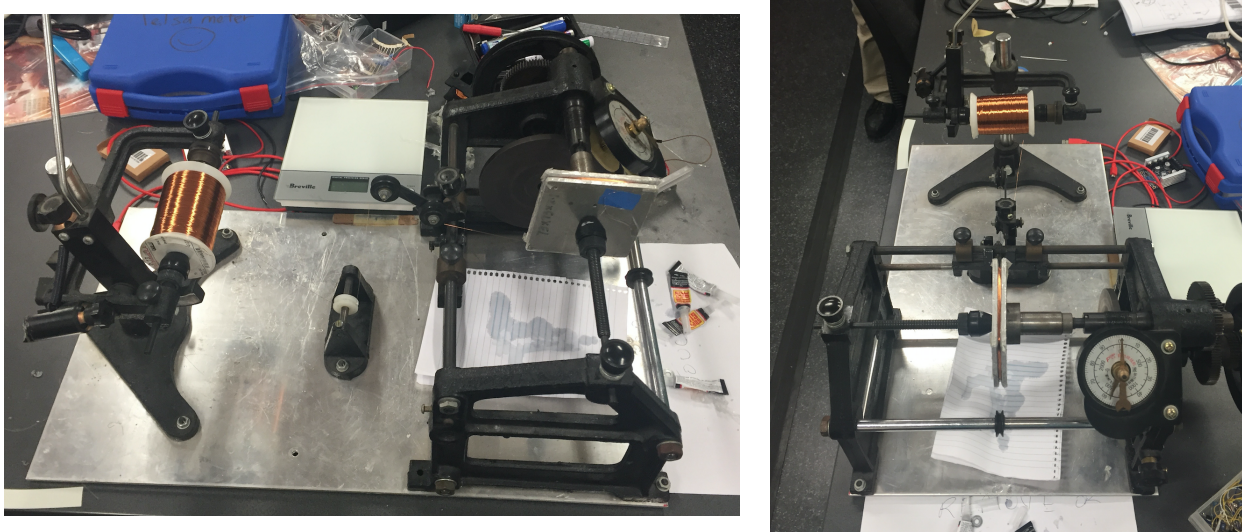
Magnetic Dipole	Number of Turns	Current	Area	Voltage	Resistance	Power Required
$0.14Am^2$	132	0.2A	$0.005329m^2$	5V	$24.9\Omega$	1W

#### 4.2.3 Construction of Magnetorquers

As mentioned previously the Magnetorquers were built in house using equipment provided in the space lab. The following procedure was applied to make each magnetorquer:

1. The metal structural mould for the magnetorquer was unscrewed and sticky tape was applied to areas that were likely to come into contact with glue.
2. The mould was placed in the winder and the copper wire was set up as shown in the photographs below.

Figure 4.3: Magnetorquer Construction Set Up



3. The wire at the very beginning of the coil was taped to the side of the mould to keep it separate from the coil so that it can be connected to the PCB.
4. In order to measure the number of turns, the counter on the winder was set to zero.
5. Twenty turns were completed and then a layer of super glue was added to the coiled wire on all four sides in order using a thin brush.
6. Step 4 was repeated until the required number of turns was reached at which point another layer of glue was added to each side of the coil.
7. The copper wire was cut and the wire at the very end of the coil was not stuck to the the main coil in order to provide a connection between the PCB and the magnetorquer.
8. The glue was allowed to set for 10 mins and then the coil was carefully removed from the mould with the aid of the sticky tape.
9. Once completed the ends of coil were carefully scraped with sandpaper in order to remove the protective coating and allow current to be passed through.
10. The coil was testing by attaching it to a battery and using a compass to determine whether a magnetic field was being produced.
11. An Ohmmeter was used to determine the resistance through the coil.

After testing both magnetorquers were found to have a slightly higher resistance than predicted with the first magnetorquer reading a resistance of  $27.2\Omega$  and the second magnetorquer reading  $28.1\Omega$ . This is roughly a 10% increase on the predicted value of  $24.9\Omega$  and is most likely caused by the effect of the super glue which was not taken into consideration in the original calculations. This will result in the magnetorquers using a slightly lower current as voltage is constant and have a lower maximum dipole value. These values were calculated to be  $0.138\text{Am}^2$  and  $0.137\text{Am}^2$  for magnetorquers 1 and 2 respectively. The image below depicts magnetorquer 1 just after construction.

Figure 4.4: Completed Magnetorquer



The magnetorquer is currently designated as TRL 4 based on the NASA scale. It has been demonstrated to work in laboratory testing environment using coils of wire to model a magnetic field approximately ten times greater than that of the earth's. However the component has not yet been fully integrated with the ACS system or been tested in the space environment.

### 4.3 Control System

#### 4.3.1 Detumble Phase

The first phase of the attitude control system will be the detumble phase in the period immediately after SnapSat's launch from the spacecraft. The aim of the detumble phase is to reduce the rotation of the satellite to a near zero state. There is no required attitude, that is initialised in the second phase. Due to the high initial expected rate of tumble of 10 degrees per second, the photodiode sun sensor system will not be used in this phase. Instead data from the IMU, primarily the gyro and the magnetorquer, will be utilised to determine the pitch, roll and yaw velocities. Since, the IMU will be calibrated prior to launch it is expected that it will be most accurate during this initial phase. The system will input the gyro and magnetometer IMU data into a B-Dot Controller. The B-Dot Controller will then calculate a torque in the opposing direction that matches the rate of change of the magnetic field and output the required PWM voltage to the magnetorquers.

$$\begin{aligned}\dot{\vec{B}} &= \omega(t) \times \vec{B}(t) \\ m(t) &= -k \cdot \dot{\vec{B}}(t) \\ T_c(t) &= m(t) \times \vec{B}(t)\end{aligned}$$

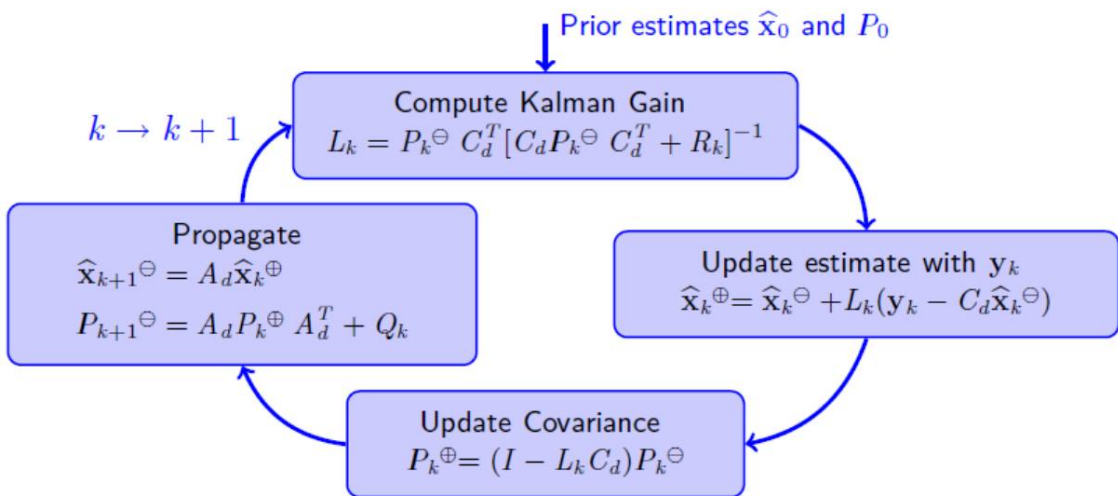
#### 4.3.2 Attitude Control Phase

After the angular velocity of the satellite decreases to a near zero value, the SnapSat will enter into the attitude control phase. This will be the long term state of the satellite and it will allow the satellite to be controlled accurately enough to fulfill the operational design and take photographs of designated cities. The control phase will take inputs from the accelerometer and photodiode sun sensor system and use them to determine the attitude of the satellite. After defining a desired attitude for the SnapSat a PID function will be used to convert the error angle into a PWM voltage

used to control the magnetorquers and drive the satellite towards the desired set point.

Raw sensor measurements can only give a rough estimation of state, so use of filtering is required for real time state estimation with minimal errors. Filtering is a method of determining the current state of the satellite based on current and past observations [?]. The extended Kalman filter will be implemented in order to handle the non-linear dynamics involved in spacecraft attitude estimation. The extended Kalman filter "predicts the new state estimate based on previous data and then updates the result with the new observations" [?]. Below is a diagram of the method by which the Kalman filter is implemented:

Figure 4.5: Model of Kalman Filter [?]



### 4.3.3 Single Axis Control Model

The dynamic model for the magnetorquer control system was produced by three fundamental equations:

$$T = N \cdot I \cdot A \cdot B \cdot \sin(\theta)$$

$$V = I \cdot R$$

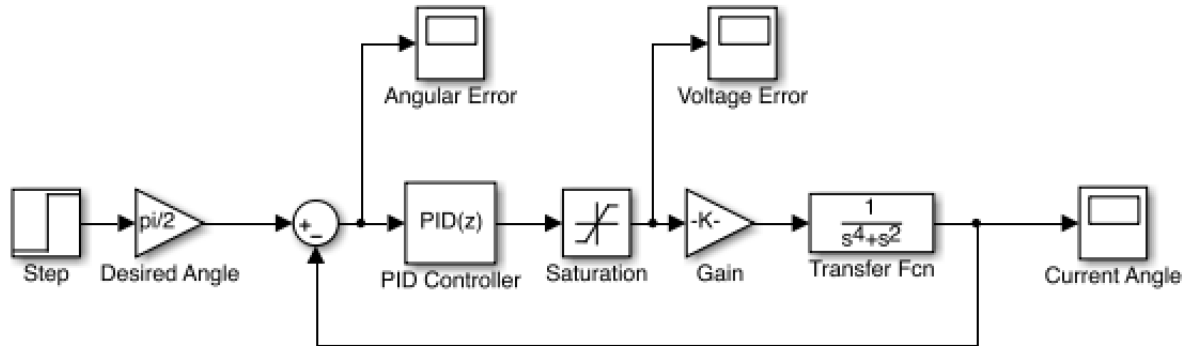
$$T = J \cdot \ddot{\theta}$$

By combining these three equations and using a Laplace transform the following dynamic model was determined:

$$\frac{\theta(s)}{V(s)} = \frac{N \cdot A \cdot B}{J \cdot R \cdot s^2 (s^2 + 1)}$$

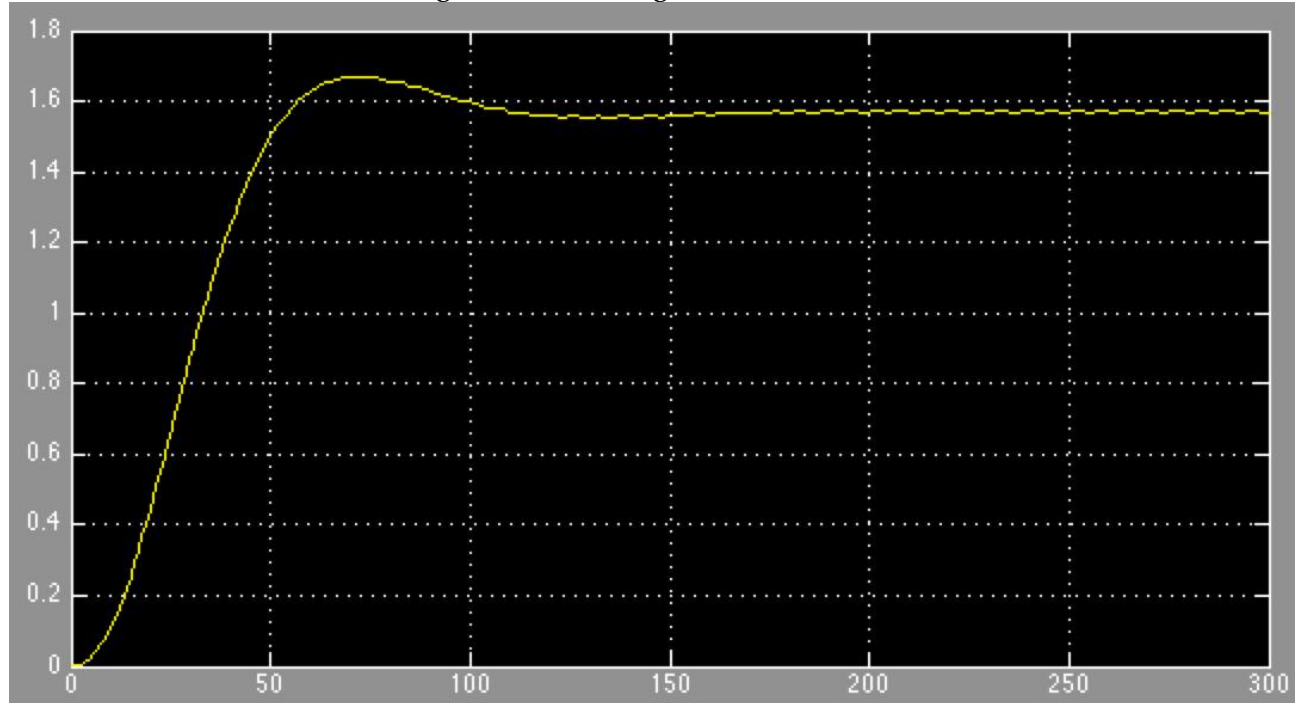
Thus using this function the following Simulink model was produced to determine the expected response of the satellite given certain inputs.

Figure 4.6: Simulink Model of Yaw Axis Control System



Using this Simulink model for a yaw input of  $90^\circ$ ( $1.57\text{rad}$ ) the response of the satellite was plotted. As can be seen in the plot below, the system has a rise time of approximately 55 seconds while settling time is around 110 seconds. Whilst there is no steady state error in the plot the angle continues to oscillate slightly in steady state.

Figure 4.7: Yaw Angle Rotation to  $90^\circ$



#### 4.4 Disturbance Torques

When in orbit there are a number of environmental forces that will result in disturbance torques and affect the attitude of SnapSat over the course of its orbit. Although these torques are minute when compared to torques experienced on earth, in space they can have a noticeable affect. Magnetic disturbance torque is a result of the interaction between the residual dipole of the on-board electronic components and the earth's magnetic field. The measured residual dipole moment of cubesats of similar size is around  $0.01\text{Am}^2$  [2]. The torque is given by the equation:

$$T_{res} = M_{res} \cdot B_{Earth}$$

There will also be a torque on the satellite as a result of the the gravity gradient, which is a function of the principle moment of inertia and the angular rate of orbit.

$$T_g = (I_{max} - I_{min}) \cdot 3n_{max}^2$$

Due to the fact that this is a low earth orbit at an altitude of 350km there is atmospheric drag force on the satellite given by the following equation:

$$F_d = \frac{1}{2}\rho v^2 C_d A(N \cdot D)$$

This drag force results in an atmospheric drag torque which is calculated by multiplying the force by the distance between the centre of aerodynamic pressure and the geometric centre which is known as the lever arm and denoted by P.

$$T_d = P \times F_d$$

Finally solar radiation pressure also implements a torque on the satellite given by the equation:

$$T_S = \frac{\phi}{c^2} A(1 + Q)(N \cdot S)d$$

Using these equations the max disturbance torques for SnapSat in orbit were estimated based on a mixture of data from SnapSat itself and other comparable satellites currently in orbit.

Table 4.2: Estimated Disturbance Torques on SnapSat

Torque Type	$N \cdot m$
Residual Dipole Torque	$3.4 \times 10^{-7}$
Aerodynamic Torque	$1.8 \times 10^{-7}$
Gravity Gradient Torque	$2.48 \times 10^{-9}$
Solar Pressure Torque	$9.86 \times 10^{-10}$
Total Disturbance Torque	$5.23 \times 10^{-7}$

As can be seen from the table, for an altitude of 350km the two largest disturbance torques are residual dipole and aerodynamic torque.

## 5 Electrical Power Subsystem

The Electrical Power Subsystem (EPS) has the function of providing power to the CubeSat. For orbital flights power comes from 1W solar cells mounted on 5 of 6 faces, which charges the CubeSat at 1W when it is exposed to direct sunlight. However, for balloon flights there is insufficient incident light on the sides of the CubeSat due to the container in which it is mounted. As a result all power comes from two 1200mAh, 3.7 V Adafruit LiPo batteries mounted in the centre of the CubeSat.

FIGURE SHOWING LOCATION OF EPS BOARD

The EPS consists of two main sections; the charging circuit, and the voltage rails.

### 5.1 Charging Circuit

The charging circuit consists of two Adafruit LiPoly chargers designed to operate in conjunction with LiPo batteries and solar panels. They automatically draw from whichever source supplies the greatest amount of power (solar panels or batteries) which eliminates the need for a switching circuit when running off battery power. The only requirement is that the solar panels must provide a minimum of 6V output power supply to overcome the threshold of the internal circuit. By using two charging circuits rather than one, the batteries can be charged separately, which simplifies the load balancing at the expense of a fuller EPS PCB as shown in figure 5.1.

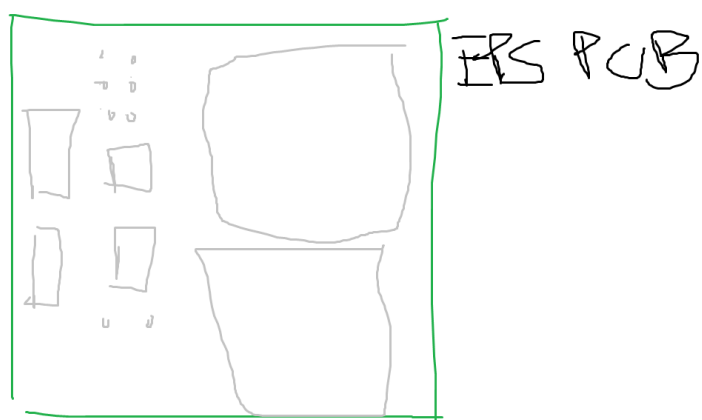


Figure 5.1: The EPS PCB. Although this PCB is full it is functional, and the extra changing circuit has not taken the place of another component.

### 5.2 Voltage Rails

Devices in this CubeSat require an even split of 3.3V and 5V power and some, the GPS in particular, require amperages above what the MCU can supply. Consequently, the EPS provides 3.3V and 5V power rails for components. However, although the MCU is a 3.3V device it is designed to run off an external supply of 6-20V, which is then transformed using an on board regulator into 5V and 3.3V. Given that, the EPS provides its own regulated 5V output which is fed directly into the Arduino's 5V pin. This has the potential to damage the MCU if done incorrectly so the margin of error for the 5V rail is extremely small.

To transform the 3.7V battery power to 3.3V and 5V rails the system uses two TI Buck Boost converters, calibrated for 3.3V and 5V respectively. These are rated to a maximum current draw of 1.5A which is sufficient to power all devices and were chosen because of their reliability and output voltage stability [5].

### 5.3 Battery Lifetime

Given that the system operates using 250 mA CHECKCHECKCHECK(depending on the precise mode of operation) it can run for 10 hours off this configuration. As a standard balloon flight is expected to last for a maximum of 4 hours CHECKCHECKCHECK this is more than sufficient to power the CubeSat for the duration of the flight.

# 6 On-Board Computer and On-board Data Handling Subsystem

The SnapSat uses an Iduino Due Pro micro controller unit (MCU) to control it's operation. It does not use an RTOS, instead using the real time clock to trigger events at pre-set times and interrupt based control to prioritize incoming messages of the communications subsystem and other time critical systems (see figure 6.2).

## 6.1 Selection

The Iduino Due Pro was chosen because it is a powerful micro controller, with a large amount of program space and sufficient peripherals to run all modules off. Additionally it has an external removable programmer, which gives it a relatively small form factor, (86.3mm by 53.3mm) allowing to fit easily within the CubeSat.

## 6.2 On-board Data Handling

The MCU interfaces with the other modules through the SPI, I2C1, I2C2, Serial0 and Serial3 peripherals, in addition to several GPIO pins as shown in figure 6.1. This leaves a Serial and NMEA module free which could easily be used to accommodate further subsystems in the future. Note that the SPI module and one of the I2C modules are shared between slave components, in such a way that more could be added to these busses in the future.

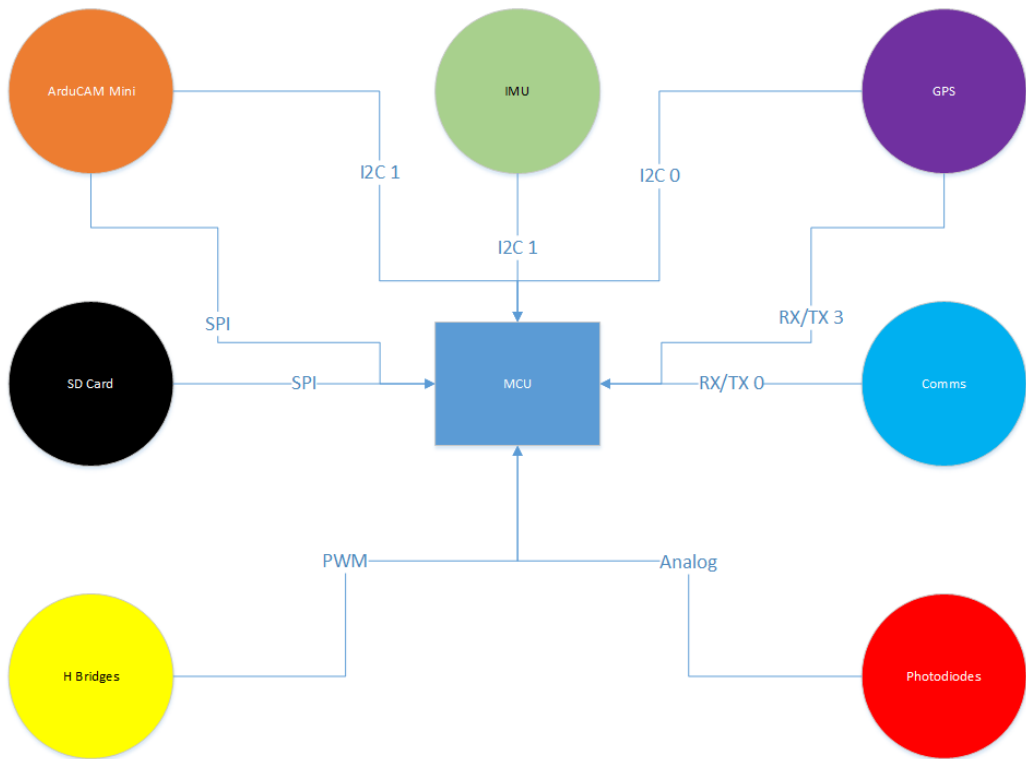


Figure 6.1: A diagram showing the interactions between the MCU and the other subsystems.

## 6.3 Modes of Operation

The CubeSat can operate in several modes of operation throughout an orbital flight, depending on the stage of flight, as laid out in the PDR and shown in figure 6.2.

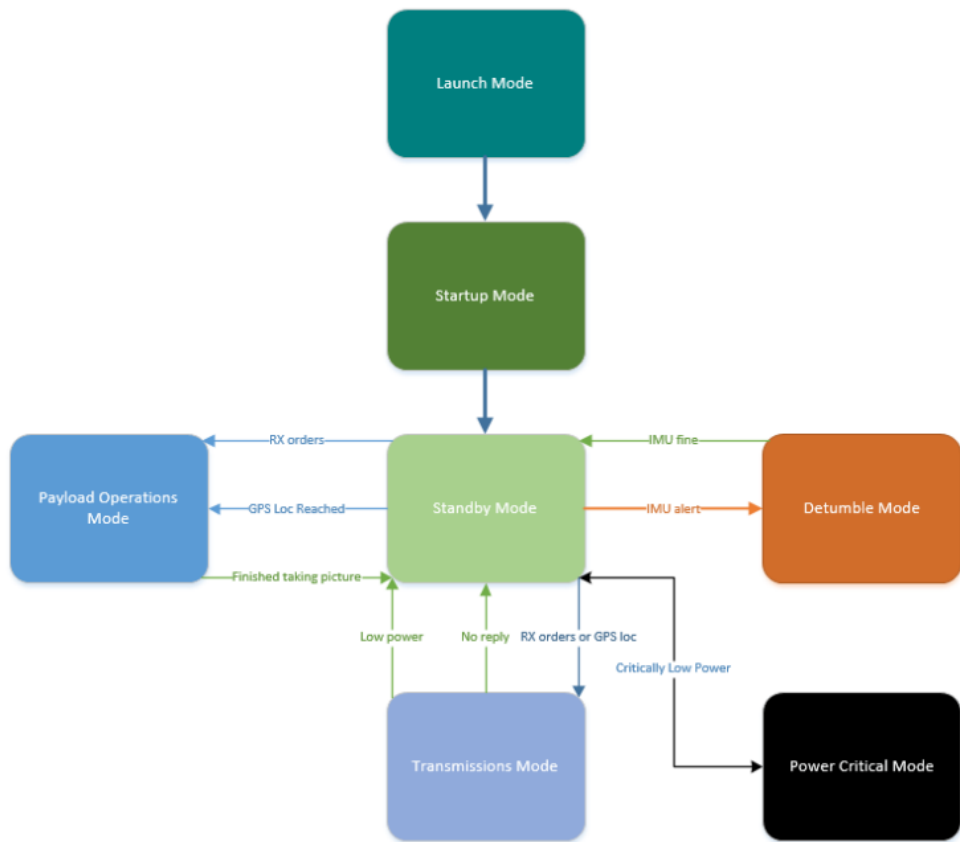


Figure 6.2: A diagram showing the modes of operation during flight.

Balloon flight, unlike orbital flights, have no CubeSat Design Specifications regarding power upon launch [6]. Consequently, SnapSat is to be launched in Standby mode while moving into Payload Operations Mode and Transmissions Mode as required. However, the CubeSat will never enter Power Critical Mode as shutting down extra systems to conserve power is ineffectual without operational solar panels or a similar means of charging.

## 7 Communications Subsystem

The communications system that was decided upon consists of a RFD 900+ transceiver that is linked to a ground station and other satellites with the same chip. The transceiver chip is connected to two antennas that increase gain allowing for larger uplink and downlink margins. The chip communicates to the OBC via UART and for a simple two node communication system works out of the box. For recovery purposes it was decided the satellites to be launched at the same time as SnapSat will be linked together via a multipoint network.

The requirements of the communication system include emitting a beacon containing the whole orbit data (WOD) collected every 30 seconds. It must also be able to accept commands from the ground station and send back payload data to earth. An example of the commands this system is able to receive and execute are turning transmissions on and off to control which satellite is emitting at a set time.

### 7.1 Components



Figure 7.1: RFD900

As mentioned above the core of the communications subsystem is the RFD 900+ transceiver from RFDesigns. It was decided that the Arduino shield used to interface the transceiver with the OBC was not necessary and direct soldering on to our PCBs would allow for a more compact design. To complete this the following pins were connected to the associated Arduino pins with data in from the transceiver connecting to data out of the Arduino and vice versa.

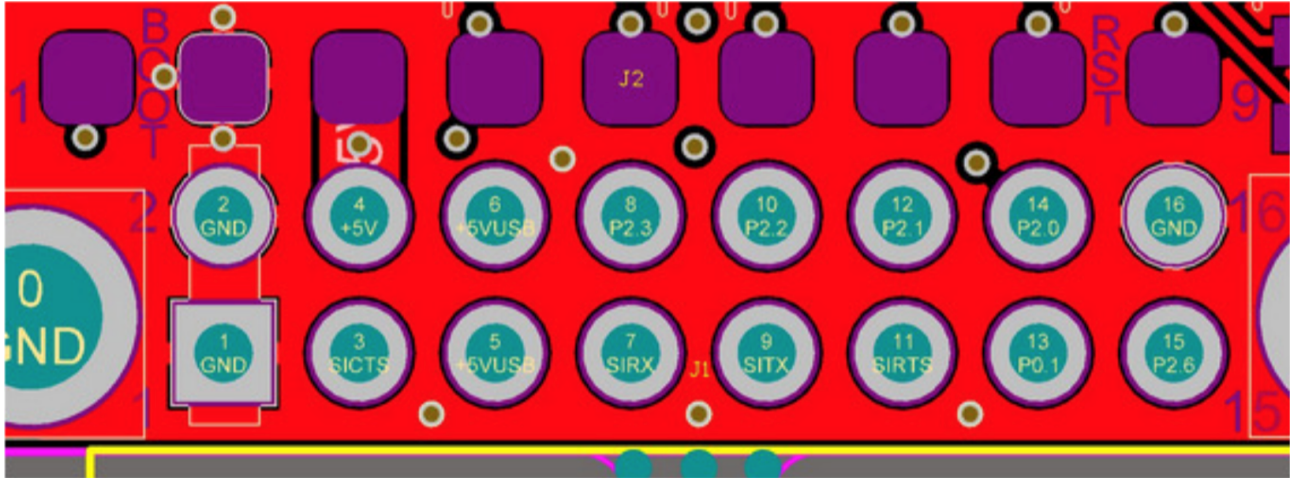


Figure 7.2: Pin Diagram

Pin	Function
1	Ground
4	Vcc
7	UART data in
9	UART data out

Figure 7.3: Table of pins used

The transceiver has a wide range of settings that can be customised for different missions and because of this is used extensively in balloon launches. The data rate ranges from 4 Kbits/s to 250 Kbits/s and this can be set or dynamically change depending on the signal. The line of sight range that will be utilised has been recorded between 40km – 60km, making it ideal for a balloon launch which normally ascends to 30km. An air speed of 64kps will give a range of about 40km depending on antenna. If the air speed is set to be lower, the range of the wireless link increases but the amount of data that you can send will be limited.

Performance	
Supported RF Data Rates (Kbits/s)	4, 8, 16, 19, 24, 32, 48, 64, 96, 128, 192 and 250
Indoor Range	500m – 1km
Line-Of-Sight Range	40km or more depending on antennas
Transmit Power	0 to 30dBm in 1dBm steps
Receiver Sensitivity	>121dBm at low data rates
Low Noise Amplifier	>20dB

The RFD900+ operates within the frequency band of 902 MHz-928MHz and uses frequency hopping spread spectrum (FHSS) to improve its immunity to interference.

Features	
Serial Data Interface	+3.3V nominal, 5V tolerant
Configuration Method	AT Commands, APM Planner, Customised Configuration Tool
Frequency Band	902MHz - 928MHz
Interference Immunity	FHSS (Frequency Hopping Spread Spectrum)
Serial Interface Data Rate	2400, 4800, 9600, 19200, 38400, 57600, 115200 baud
Antenna Options	Yagi, 1/2 Wave Dipole, 1/4 Wave Monopole Antenna
GPIO	6 pins (Digital, ADC, PWM capable)
Compliance Standards	FCC Part 15.247, AS/NZS 4268:2008

The configuration that was chosen includes a baud rate of 57600 with no parity, 8 data bits and 1

stop bit. This was chosen to maximise the data send back to the ground station whilst maintaining a solid link margin.

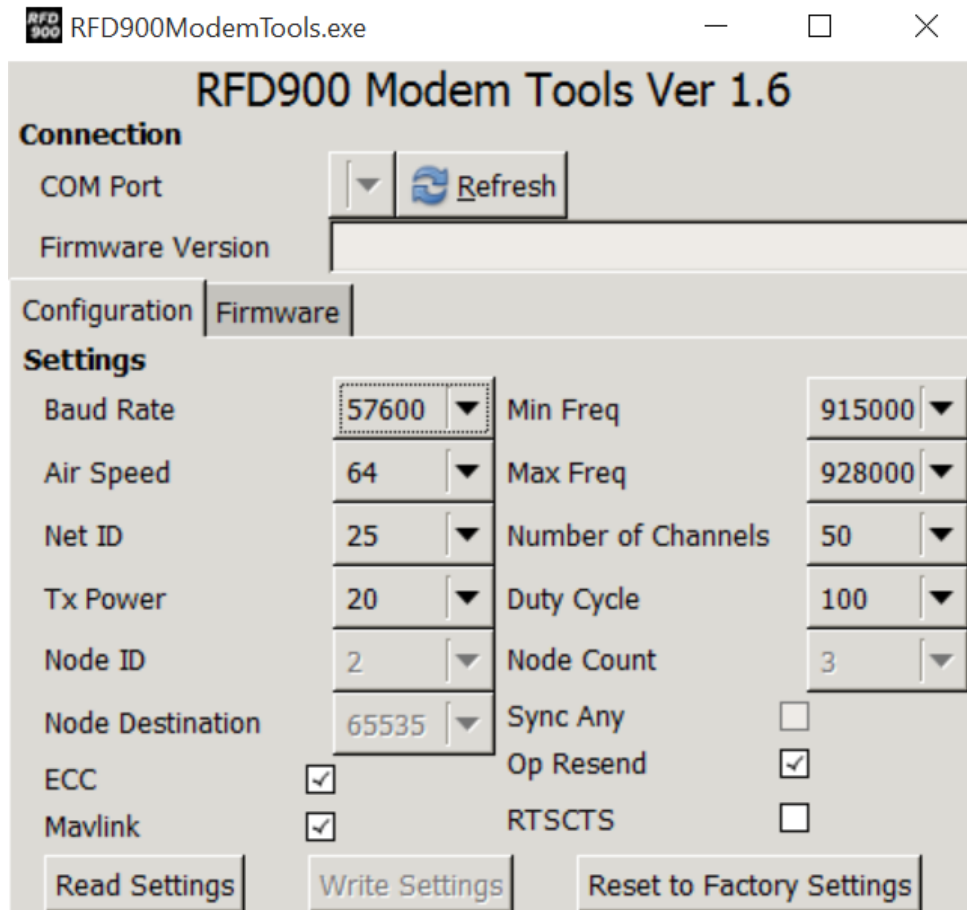


Figure 7.4: Settings used with transciever

To increase the gain on both ends of the transmission, different antennas will be used at the ground station compared to the satellite. At the ground station we will utilise a yagi antenna. Yagi antennas are recommended for Ground-Station applications due to their size. They have approximately 6dBi gain and give significant link budget improvement when compared to standard dipole, or monopole antennas. On the satellite we will use two quarter wave antennas. The choice was between this and half wave dipole antennas but the quart wave was declared superior due to its small size. Quarter Wave Monopole Antennas are recommended for air-borne, or space constrained applications. They are required to be mounted on a ground plane of approximately 20cm diameter or more to operate as intended.



Figure 7.5: Quarter Wave Monopole Antenna

The RFD900 has two antenna ports and firmware which supports diversity operation of antennas. During the receive sequence the modem will check both antennas and select the antenna with the best receive signal. In the case of only one antenna connected, it will automatically select the port with the antenna connected. Testing by Silicon Labs has shown that link budgets can be improved in the order of 6-8dB by employing a diversity scheme.

Polarisation diversity is the case where the antennas are perpendicular to each other. i.e. one vertical, and one horizontal. This is effective in reducing multipath effects which affect one or the other polarisation. We will utilise this principle and set the antennas at a 90-degree angle to each other.

The RFD900 can be implemented in either simple pair between two nodes or a multipoint network. In our case we have opted to use the multipoint network to allow the satellites to communicate in the air, relaying their position to aid in recovery. The following is an example of a 5 node network that will be ideally implemented. The network consists of Node 0, the ground station, Node 1, the mother satellite, and the remaining nodes are the other satellites. This structure has not been confirmed as the satellites participating in the launch is yet to be decided.

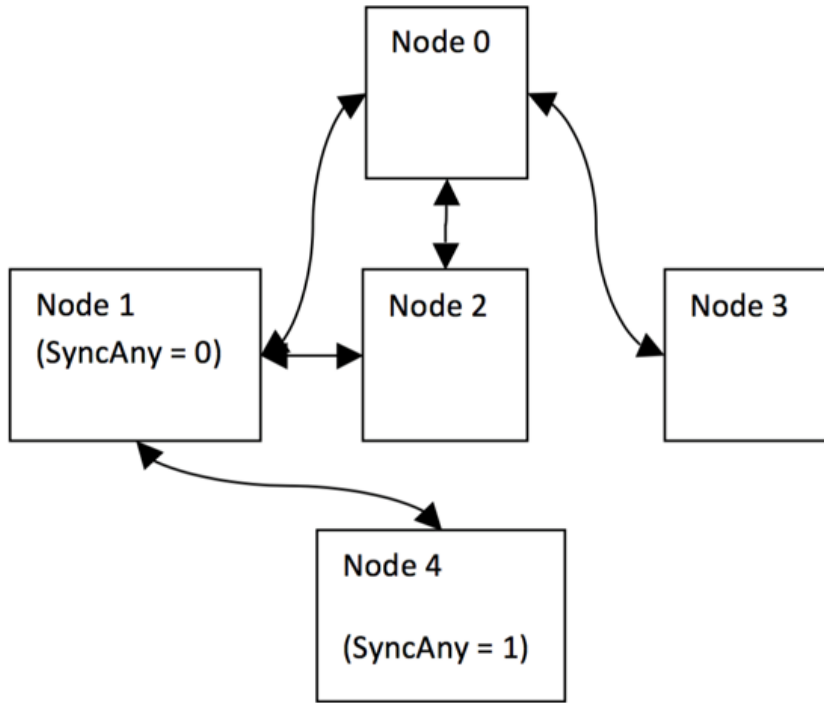


Figure 7.6: Five-node Network Setup

**Ground Station** Mobile ground station utilizing the same model rfd900+ transceiver connected to a yagi antenna. Yagi antennas are recommended for Ground-Station applications due to their size. They have approximately 6dBi gain and give significant link budget improvement when compared to standard dipole, or monopole antennas.

The system has been set up to receive a number of commands from the ground station and act upon them. This allows it to be controlled by an operator and gives it superior functionality. The list of commands is as follows:

#### User Commands

1. SET/GET TRANSMIT ON/OFF - Sets transmit to on or off
2. SET/GET MODE [mode] - Sets the mode of the satellite
3. DOWNLOAD PAYLOAD - Download all scientific data that hasn't been sent yet
4. SET PICTURE RATE - Set how often pictures are taken
5. SET [variable] [value] - Change the value for specific variables in code
6. RESET - Causes the device to reset
7. DELETE [date] - delete data before the given date

## 7.2 Link Budget Summary

After calculating the link budget for the satellite in orbit we now have a much larger factor of safety as the free space path loss is reduced by 21 dB to 101 dB, giving us a larger margin, even considering

the change in transceiver. The RFD 900+ has been used numerous times successfully for balloon launch, thereby confirming the margin is adequate. The assumptions made with the link budget include clear sky with normal humidity and a temperature of 30 degrees Celsius.

<b>Uplink Budget</b>	
<b>Transmitter: Ground Station</b>	<b>Receiver: SnapSat</b>
Required $E_b/N_0$	56.1 dB
Threshold $E_b/N_0$	23.2 dB
<b>System Link Marking</b>	32.9 dB

Figure 7.7: Uplink budget

<b>Downlink Budget</b>	
<b>Transmitter: SnapSat</b>	<b>Receiver: Ground Station</b>
Required $E_b/N_0$	26.07 dB
Threshold $E_b/N_0$	20.5 dB
<b>System Link Marking</b>	15.56 dB

Figure 7.8: Downlink budget

## 8 Thermal Control Subsystem

The method of developing thermal control used for SnapSat considers the following simplified model of the satellite. The main body is idealised as a system dissipating heat (located at the centre of the CubeSat) to the boundary located on the face of the CubeSat. This boundary is exposed to the outer environment. Energy conservation laws require that in steady state, the heat dissipated by the internal electronics is equal to that transferred to the boundary. Thus, the heat from internal dissipation added to the heat adsorbed from the outside is equal to the heat rejected to space. The general governing equation is

$$Q_{1 \rightarrow 2} = K_{1 \rightarrow 2}(T_a - T_2) \quad (8.1)$$

Where  $Q$  = heat exchange (Watts)

$K$  = proportionality factor constant (Watts/Kelvin)

$T$  = temperature of bodies (Kelvin)

between bodies 1 and 2. Additionally, the heat radiated from a blackbody surface of temperature  $T$  is given by

$$Q_r = KT^4 \quad (8.2)$$

Where the proportionality factor depends on physical constants, the material properties, surface conditions and geometry. A schematic of the incoming thermal radiation on the CubeSat in Low-Earth Orbit (LEO) is shown below.

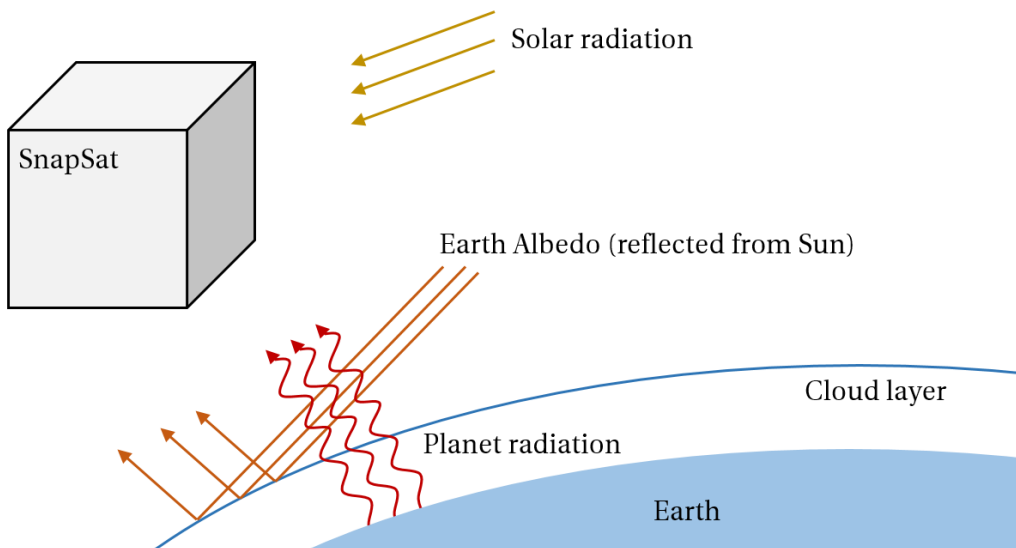


Figure 8.1: Incoming thermal radiation on the satellite

### 8.1 The Three Modes of Heat Transfer

The first law of thermodynamics states that the internal energy change on a system is equal to the amount of heat added subtracted by the amount of work done. The work done by the satellite on its environment is zero in our case, so the change in energy becomes

$$\frac{dU}{dt} = Q = A \rho c_p \frac{dT}{dt} dx$$

Where  $Q$  = heat added (Watts)  
 $A$  = cross-sectional area ( $\text{m}^2$ )  
 $\rho$  = density of material ( $\text{kg}/\text{m}^3$ )  
 $c_p$  = specific heat capacity ( $\text{J}/\text{kg K}$ )  
 $T$  = temperature (K)  
 $dx$  = incremental length (m)

Is is dependent on the physical and geometric properties of the satellite and the change in temperature. The total heat balance for the satellite is then given by the heat flux entering the system minus the flux leaving the system. These are characterised by the modes of heat transfer below.

### 8.1.1 Convection

Convection is the heat transfer between a solid surface and flowing fluid. This is of importance during mission launch, however does not apply in a space environment. Convection considerations were ignored for this design.

### 8.1.2 Conduction

Thermal energy transfer within a material due to vibrating atoms - for example if the material is heated in one location, conduction is the method by which it spreads to the rest of the material. This is most important for on-board electronics, the rate of heat transfer is given by

$$Q_{conduction} = \frac{kA}{\Delta x}(T_1 - T_2)$$

which is the same as equation 8.1. The heat transfer depends on the area of the satellite normal to the direction of heat transfer  $A$ , the thermal conductivity  $k$  and the temperature differential  $T$ .

### 8.1.3 Radiation

Perhaps the most complex form of heat transfer is radiation, where all bodies above 0K emit and absorb electromagnetic energy. We consider each body as a perfect emitter (black body) and integrate the emitted energy across all wavelengths, this gives

$$E_{bb} = \epsilon\sigma T^4 \quad (8.3)$$

measured in  $\text{Watts}/\text{m}^2$ . This is the same as equation 8.2, where  $\sigma$  is the Stefan-Boltzmann constant. In this case, the emissivity  $\epsilon$  has been added to account for the fact that the surfaces are not perfect black bodies.

## 8.2 Total Incoming Radiation

The total radiation incoming onto the satellite as it orbits is defined in figure 8.2 below. This assumes that the satellite is in full view of the sun 65% of the time in each orbit.

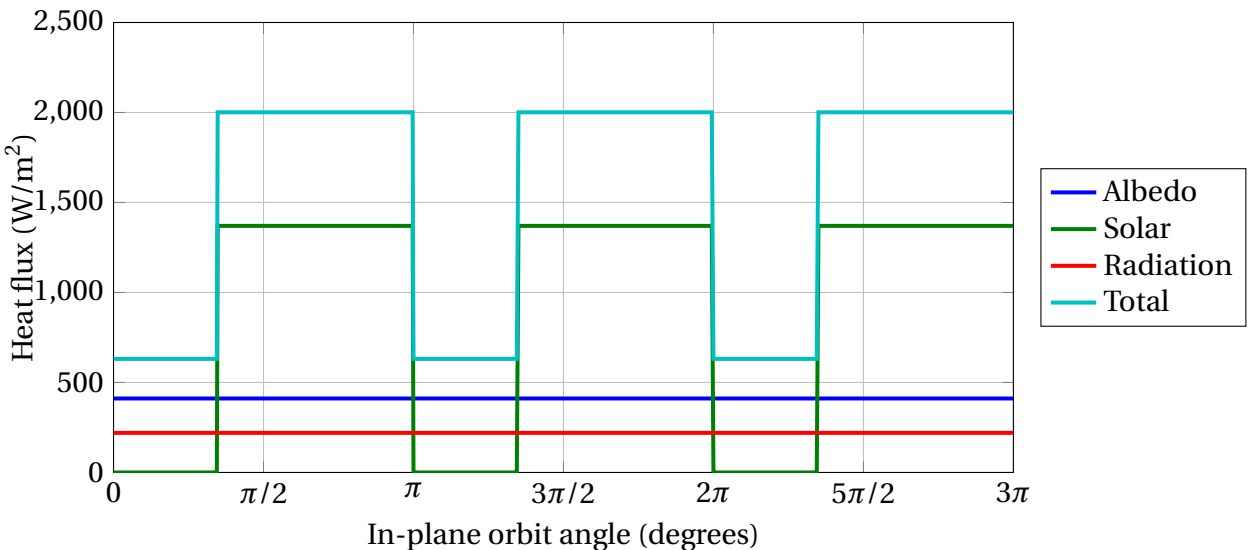


Figure 8.2: Radiation incoming onto the satellite as it orbits

Whilst this is the incoming radiation on the satellite as a whole, it is not indicative of the amount of radiation received by each side of the satellite. As the spacecraft is attitude controlled, the lower side will be facing the Earth always and only receive solar radiation for a short period of time. The amount of solar radiation (and even Earth IR radiation) received depends on the projected area that the radiation falls upon. Corrections are found using the view factor of each side of the satellite.

### 8.2.1 View Factors

The view factor of each side of the satellite allows for the calculation of the effect of the incoming radiation. The calculation takes into account the projected amount of heat flux on each side. The view factor is of importance when considering the radiation effect of Earth's infrared and albedo. The view factor indicates the area of the panel that radiation falls upon. The formulae to obtain the view factors for each panel is

$$F_{i \rightarrow j} = \frac{1}{A_i} \int_{A_i} \int_{A_j} \frac{\cos\theta_1 \cos\theta_j}{\pi S^2} \quad (8.4)$$

Where  $S$  is the shape factor. Whilst this a complex equation (especially for complex geometries), the view factors for a simple cubesat orbiting a sphere (Earth) are

$$V_F = \frac{\cos\gamma}{H} \quad (8.5)$$

If the panel is facing towards Earth such that the whole surface can be 'seen' by the panel. However if the panel is not facing the Earth

$$V_F = 0 \quad (8.6)$$

If the panel is oriented in such a way that it is only partially oriented to see the Earth then

$$V_F = \frac{1}{2} - \frac{1}{\pi} \sin^{-1} \left( \frac{(H^2 - 1)^{1/2}}{H \sin \gamma} \right) + \frac{1}{\pi H^2} \cos \gamma \cos^{-1}(-(H^2 - 1)^{1/2} \cot \gamma) \quad (8.7)$$

$$- \frac{1}{\pi H^2} (H^2 - 1)^{1/2} \times (1 - H^2 \cos^2 \gamma)^{1/2} \quad (8.8)$$

Where  $\gamma$  is the angle between the normal to the Earth's surface (or normal to the projected disk that the satellite panel sees) and the normal to the panel. [7]

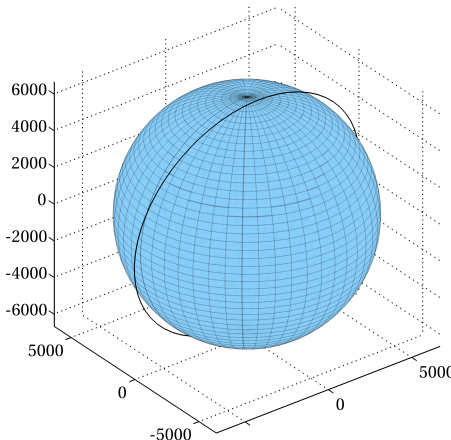


Figure 8.3: Representation of Satellite Orbit

### 8.3 Spacecraft Thermal Environment

As shown in figure 8.1, the spacecraft is subject to the following heating mediums: solar radiation, Earth infra-red and Earth albedo. The amount of radiation falling upon each panel is a function of the surface absorptivity and the view factor of the panel. The panel naming convention for this section is shown below.

#### 8.3.1 Solar Radiation

The incoming solar radiation on the satellite is given by

$$Q_{solar} = Q_{sun} \alpha \cos \phi \quad (8.9)$$

Where  $Q_{sun} = 1350$  solar heat flux ( $\text{W/m}^2$ )

$\alpha$  = panel surface absorptivity

$\phi$  = angle between the normal of the panel to the sun (rad)

For each of the panels, the solar radiation intensity is shown in the figure below. The skew in four of the panels is due to the  $45^\circ$  rotation of the orbit along the  $z$  Earth frame.

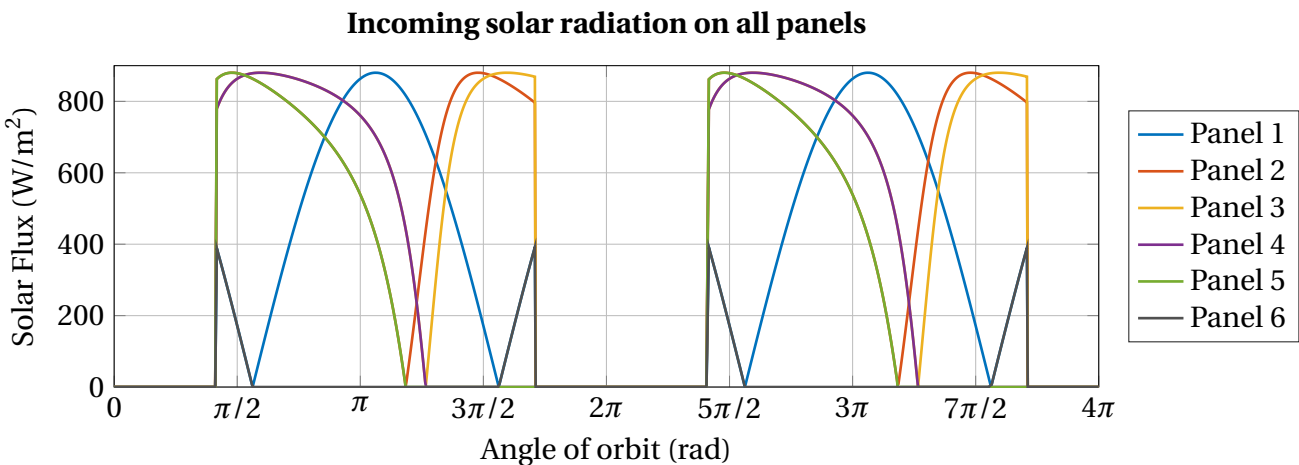


Figure 8.4: Solar radiation falling on each panel

### 8.3.2 Earth Infrared Radiation

The incoming radiation from the Earth is in the infrared band. This radiation is due to the effective temperature of the Earth and is a constant value for each panel. For this reason, the values will not be displayed on a graph. The incoming radiation varies from panel to panel depending only on the view factors as described in section 8.2.1. The value is given by

$$Q_{Earth-IR} = \sigma T_{Earth}^4 \alpha F_V \quad (8.10)$$

Where  $\sigma = 1.381 \times 10^{-23} \text{ m}^2 \text{ kg s}^{-2} \text{ K}^{-4}$  (Boltmann constant)

$T$  = effective temperature of the Earth

$\alpha$  = panel surface absorptivity

$F_V$  = panel view factor

### 8.3.3 Earth Albedo

The final source of external radiation is the Earth albedo, which is solar radiation that has been reflected off the Earth's could layer. The value as the cubesat orbits the Earth is given by

$$Q_{Earth-albedo} = Q_{sun} F_A \alpha F_V \cos\theta \quad (8.11)$$

Where  $Q_{sun} = 1350 \text{ W/m}^2$  (solar radiation)

$F_A$  = albedo view factor

$\alpha$  = panel surface absorptivity

$F_V$  = panel view factor

$\theta$  = angle between the spacecraft panel surface and the Sun (8.12)

The figure below shown the variation in albedo that three panels see throughout the orbit. Since each panel is not double sided, the plot cycles between two opposite panels. For instance, the orange line shown the albedo incoming on both panels 2 and 5 (the panel on the opposite side). Half of the cycle representing each panel.

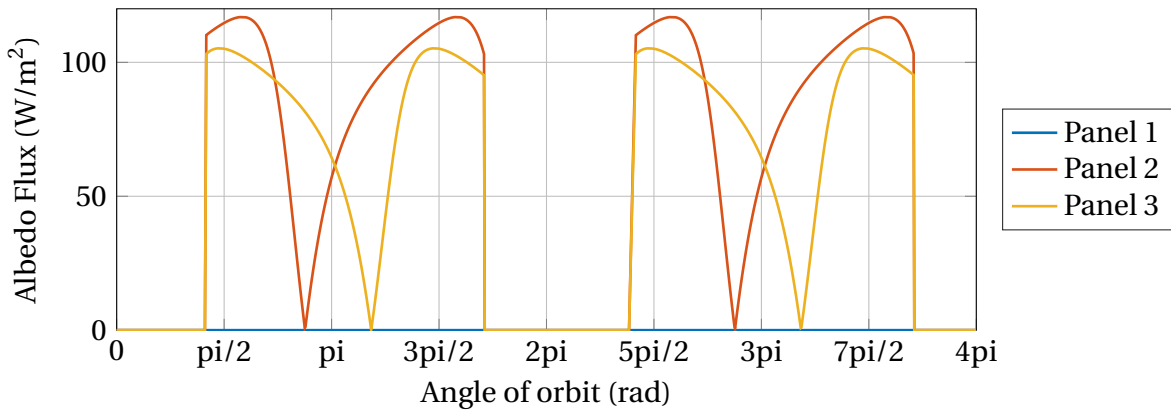


Figure 8.5: Reflected albedo falling on each panel

#### 8.3.4 Total Incoming Radiation Per Panel

For illustration purposes, figure 8.6 shows the total incoming radiation on panel 2. This calculation was performed for all six panels.

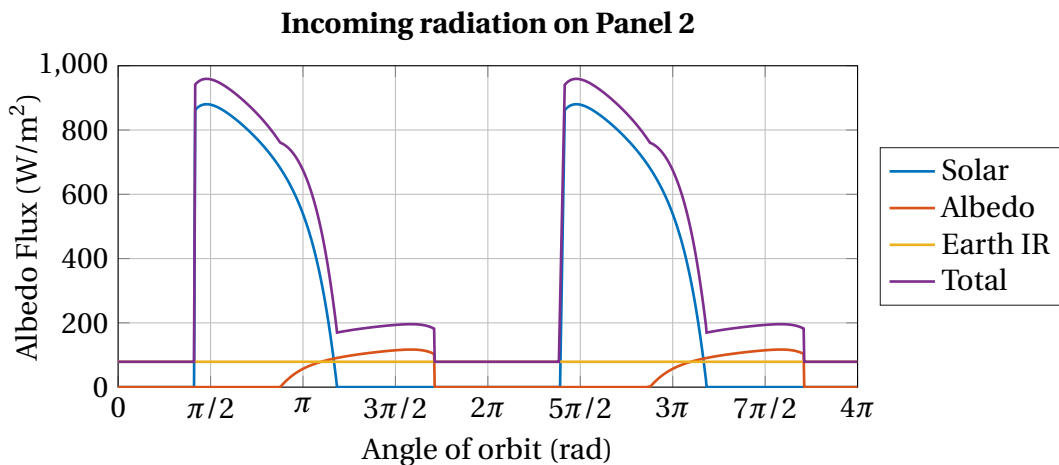


Figure 8.6: Total radiation falling upon panel 2

## References

- [1] J. Springmann, *Satellite Altitude Determination with Low Cost Sensors*. PhD thesis, University of Michigan, 2013.
- [2] D. Miller, “Mxl tech memo,” 2013.
- [3] J. Springmann and J. Cutler, “Photodiode placement and algorithms for cubesat attitude determination,” 2012.
- [4] S. Leake, “Goddard dynamic simulator coarse sun sensor model,” 2012.
- [5] Texas Instruments, *1.5-A Peak Boost/Buck/Inverting Switching Regulators*, December 2004.
- [6] R. Munakata, “Cubesat design specification,” 2009.
- [7] H. Heidt, J. Puig-Suari, A. Moore, S. Nakasuka, and R. Twiggs, “Cubesat: A new generation of picosatellite for education and industry low-cost space experimentation,” 2000.
- [8] P. Reiss, “New methodologies for the thermal modelling of cubesats,” 2012.

## A Link Budgets

Table 5.4: Uplink Budget

<b>Information on the System</b>	
<b>Transmitter: Ground Station</b>	
Orbit Altitude: 350km	
Slant Range: 652.5km	
Demodulation Method: AFSK	
Antenna Type (TX): Cross Yagi	
<b>Transmitter System (Ground Station)</b>	
Ground Station Transmitter Power Output	100 W
Ground Station Total Transmission Line, Losses	20 dBW
Ground Station Antenna Gain	3.4 dB
Ground Station ERIP	18.9 dBi
<b>Down Link Path</b>	
Free-Space Path Loss	35.5 dBW
Satellite Antenna Pointing Loss (10°)	132 dB
Ground Station Antenna Pointing Loss (10°)	10.6 dB
Satellite Transmission Line Losses	2.7 dB
Atmospheric Loss (30°)	0.5 dB
Ionspheric Loss	0.4 dB
Rain Loss	0.4 dB
Total Loss	0 dB
	146.6 dB
<b>Receiver System (on SnapSat)</b>	
Antenna Gain	2.7 dBi
Effective Noise Temperature at Space (350K/Day)	1345K
Figure of Merit (G/T <sub>a</sub> )	-28.6 dB/K
Carrier to Thermal Noise Ratio (C/T)	-136.6 dB
Boltzmann's constant (K)	-228 dBW/K/Hz
Carrier to Noise Density Ratio (C/No)	88.9 dB/Hz
<b>Modulation Process</b>	
System Desired Data Rate	1200 bps
<b>Demodulation Method Selected</b>	
System Allowed or Specified Bit-Error Rate	AFSK 1.00E-04

Table 5.5: Downlink Budget

### Information on the System

#### Transmitter - SnapSat

Orbit Altitude ≈ 350km  
 Slant Range ≈ 652.5km  
 Demodulation Method ≈ BPSK  
 Antenna Type (TX) ≈ Dipole

#### Transmitter System (SnapSat)

Satellite Transmitter Power Output	0.5 W
Satellite Total Transmission Line Losses	-3.01 dBW
Satellite Antenna Gain	0.5 dB
Satellite ERIP	2.7dBi

#### Down Link Path

Free-Space Path Loss	132 dB
Satellite Antenna Pointing Loss (10°)	10.6 dB
Ground Station Antenna Pointing Loss (10°)	2.7 dB
Ground Station Transmission Line Losses	1.8 dB
Atmospheric Loss (30°)	0.4 dB
Ionspheric Loss	0.8 dB
Rain Loss	0 dB
Total Loss	146.4 dB

#### Receiver System (Ground Station)

Antenna Gain	14.4 dBi
Effective Noise Temperature at Sydney (350K/Day)	610.1 K
Figure of Merit (G/T <sub>a</sub> )	13.5 dB/K
Carrier to Thermal Noise Ratio (C/T)	-160.71 dB
Boltzmann's constant (K)	-228.6 dBW/K/Hz
Carrier to Noise Density Ratio (C/No)	67.89 dBHz

#### Modulation Process

System Desired Data Rate	9600 bps
Demodulation Method Selected	BPSK
System Allowed or Specified Bit-Error Rate	1.00E-04
Demodulator Implementation Loss	2 dB

#### Link Performance

Required Eb/No	26.07 dB
----------------	----------

Cubesat Design Overview Report

#### Receiver - Ground Station

Elevation ≈ 30 degrees
Weather ≈ Clear Sky
Cable Length ≈ 20m
Antenna Type ≈ Cross Yagi

#### System Link Margin

**15.56 dB**